

---

# Is Complex Training Necessary for Long-Tailed OOD Detection? A Re-think from Feature Geometry

---

**Ningkang Peng**  
Nanjing Normal University

**Xuanming Chen**  
Nanjing Normal University

**Yanhui Gu**  
Nanjing Normal University

## Abstract

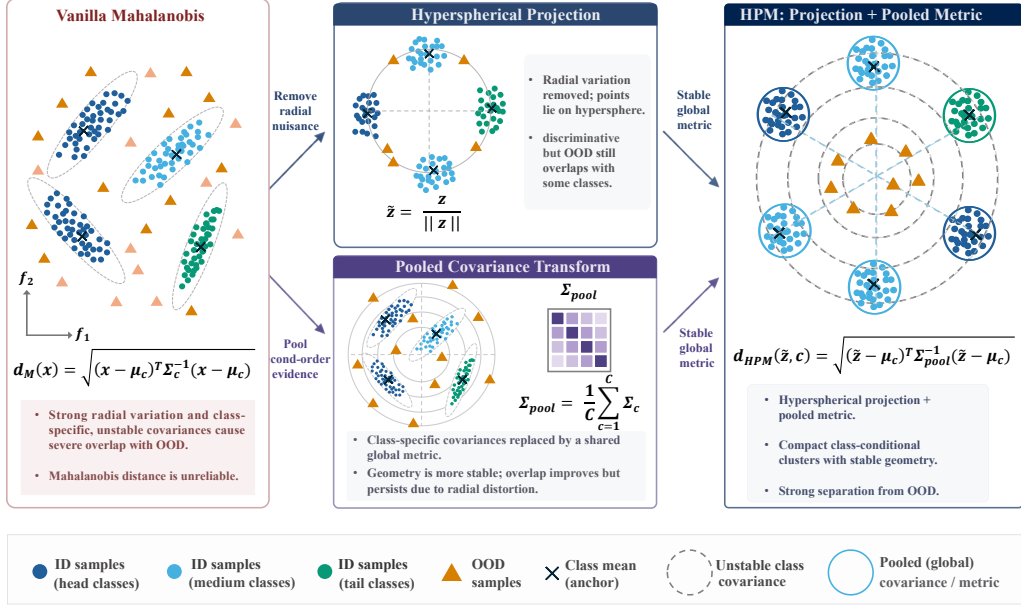
Long-tailed out-of-distribution (LT-OOD) detection is often addressed with specialized training, including auxiliary out-of-distribution (OOD) data, abstention heads, contrastive objectives, energy losses, or gradient-conflict control. We show that these training mechanisms can obscure a simpler issue: frozen long-tailed representations may already contain useful OOD evidence, but raw Mahalanobis distance is distorted by frequency-coupled feature radius and poorly supported tail covariance. We propose *Hyperspherical Pooled Mahalanobis* (HPM), a post-hoc detector that normalizes features onto the unit sphere and replaces class-specific covariance with a pooled, ridge-regularized metric while keeping class means as semantic anchors. In CIFAR-LT experiments and an ImageNet-100-LT near-OOD boundary analysis, HPM improves raw Mahalanobis scoring; for Prior-Calibrated ERM (PC-ERM), it raises AUROC from 46.49 to 85.67 on CIFAR-10-LT and from 50.40 to 78.35 on CIFAR-100-LT. This simple PC-ERM+HPM pipeline also achieves the best Log Efficiency Score (LES; 3.08) on CIFAR-100-LT, retaining roughly 95% of the best CIFAR-100-LT AUROC observed among the compared post-hoc scores at substantially lower training-time cost. These results argue for evaluating representation quality, detector geometry, and training complexity as separate factors in LT-OOD detection.

## 1 Introduction

Open-world recognition may do more than name the classes seen during training. A deployed system also needs to recognize when an input falls outside the in-distribution (ID) training distribution [Hendrycks and Gimpel, 2017, Liang et al., 2018, Lee et al., 2018]. This requirement is especially sharp in long-tailed domains such as autonomous perception, medical triage, ecological monitoring, and industrial inspection, where rare ID categories and novel hazards coexist. Long-tailed out-of-distribution (LT-OOD) detection therefore asks for two behaviors at once: retain rare known classes and reject inputs from outside the training distribution.

Because head classes provide dense supervision while tail classes may have only a few examples [Liu et al., 2019, Cao et al., 2019], many recent LT-OOD methods respond by making training more specialized. Some use energy-based objectives [Liu et al., 2020] or auxiliary outlier exposure [Hendrycks et al., 2019]; others introduce contrastive tail-OOD separation [Wang et al., 2022b], abstention or calibrated outlier classes [Wei et al., 2024, Miao et al., 2024a], adaptive outlier distributions [Miao et al., 2024b], gradient-conflict mitigation [Zhang et al., 2025], or semantic tail prioritization [He et al., 2025]. These methods have advanced the benchmark, but they raise a basic question: is increasingly complex training necessary for strong LT-OOD detection, or can a simple long-tail classifier already be competitive when the detector uses its representation properly?

We study this question through Prior-Calibrated ERM (PC-ERM), a simple baseline trained with cross-entropy and long-tail prior calibration [Menon et al., 2021]. PC-ERM uses no auxiliary OOD data, abstention head, contrastive objective, or specialized rejection loss. To compare accuracy with cost, we also report a Log Efficiency Score (LES), which relates the strongest post-hoc OOD



**Mechanism of Hyperspherical Pooled Mahalanobis**

Figure 1: HPM **geometry repair**. Class-conditional Mahalanobis is unstable when tail classes lack residual support (top path). HPM first projects features to the hypersphere to remove radial bias correlated with imbalance, then uses pooled residual covariance to replace tail-specific spectra with shared, ridge-regularized geometry while preserving class mean anchors.

AUROC of a trained model to its training time. LES separates absolute OOD performance from compute-normalized performance.

Our experiments point to a different bottleneck: raw Mahalanobis detection reads long-tailed features through an unstable geometry. Feature radius can be coupled with class frequency, so raw distance mixes semantic displacement with a training-frequency artifact. Tail classes also have too few samples to support class-specific covariance, making the estimated precision low-rank, ill-conditioned, and sensitive to regularization. Thus a simple classifier may look weak under raw distance not because its representation is unusable, but because the post-hoc metric is distorted.

We propose *Hyperspherical Pooled Mahalanobis* (HPM), a minimal post-hoc detector that repairs this geometry. It maps features onto the unit hypersphere to remove frequency-coupled radius, then replaces unsupported class-specific covariance with a pooled ridge covariance. Class means remain semantic anchors, while second-order geometry is estimated from shared within-class residuals. Figure 1 summarizes the mechanism. HPM changes only the detector: it adds no outlier head, auxiliary OOD supervision, model retraining, or specialized training objective.

HPM also complements classifier-score diagnostics. Energy and maximum softmax probability (MSP) depend only on classifier outputs, so they cannot respond to feature variation that leaves logits unchanged. This classifier-null blind spot is not our main claim, but it explains why post-hoc LT-ODD evaluation should not rely on classifier scores alone. A repaired feature-space metric can expose evidence that raw Mahalanobis distorts and classifier scores cannot observe.

Our evaluations on CIFAR-10-LT, CIFAR-100-LT, and ImageNet-100-LT use representations from recent LT-ODD and long-tail methods including PATT [He et al., 2025], PASCL [Wang et al., 2022b], AdaptOD [Miao et al., 2024b], COCL [Miao et al., 2024a], EAT [Wei et al., 2024], and DARL [Zhang et al., 2025]. On PC-ERM, HPM raises raw Mahalanobis AUROC from 46.49 to 85.67 on CIFAR-10-LT and from 50.40 to 78.35 on CIFAR-100-LT. PC-ERM+HPM also achieves the highest CIFAR-100-LT LES (3.08), retaining roughly 95% of the best CIFAR-100-LT AUROC observed among the compared post-hoc scores at substantially lower training-time cost. ImageNet-

100-LT acts as a boundary analysis of how far stabilized Mahalanobis geometry can repair the raw feature-space detector.

Our contributions are:

- We revisit whether increasingly complex training is necessary for LT-OOD detection, and use LES to evaluate OOD performance together with training-time cost.
- We identify two geometric reasons why raw Mahalanobis fails under long-tailed representations: frequency-coupled feature radius and poorly supported tail-class covariance estimation.
- We propose HPM, a post-hoc Mahalanobis repair based on hyperspherical projection and pooled ridge covariance, showing that simple PC-ERM models can achieve strong and efficient OOD detection without auxiliary OOD supervision or retraining.

## 2 Related Work

**Post-hoc OOD detection and Mahalanobis geometry.** Classical post-hoc OOD detectors score softmax confidence [Hendrycks and Gimpel, 2017], use input preprocessing or temperature scaling [Liang et al., 2018], or measure feature-space density with Mahalanobis distance [Lee et al., 2018]. Energy scoring [Liu et al., 2020] has become a strong classifier-score baseline, while later detectors exploit feature clipping, nearest neighbors, residual subspaces, or feature compactness [Sun et al., 2021, 2022, Wang et al., 2022a, Sehwag et al., 2021, Ming et al., 2023]. Our work is closest to Mahalanobis-style detection and recent feature-normalized variants [Müller and Hein, 2025], but studies a different failure mode: under long-tailed training, raw feature radius is frequency-coupled and tail classes cannot support reliable class-specific covariance.

**Long-tailed recognition and LT-OOD detection.** Long-tailed recognition has been addressed through re-weighting, re-sampling, margin adjustment, logit adjustment, contrastive learning, and decoupled training [Cao et al., 2019, Kang et al., 2020, Menon et al., 2021, Ren et al., 2020, Zhu et al., 2022, Li et al., 2022]. LT-OOD detection adds the open-set requirement that rare ID samples remain accepted while unknown samples are rejected. Recent methods improve this setting with contrastive tail-OOD separation, abstention or calibrated outlier classes, adaptive outlier distributions, gradient-conflict mitigation, and semantic tail prioritization [Wang et al., 2022b, Wei et al., 2024, Miao et al., 2024a,b, Zhang et al., 2025, He et al., 2025]. These approaches mainly change training. We ask how far a stable post-hoc geometry can take simple long-tail training before adding more specialized objectives.

**Auxiliary OOD supervision and representation geometry.** Outlier exposure can greatly improve OOD detection when suitable auxiliary data are available [Hendrycks et al., 2019], but it also couples OOD rejection with the learned ID geometry. This coupling is especially delicate in long-tailed learning, where head and tail classes receive very different statistical support. Our analysis connects LT-OOD behavior to classifier-null scatter, feature radius, covariance spectra, and effective rank, complementing studies of feature geometry and neural collapse [Papayan et al., 2020, Kornblith et al., 2019].

## 3 Preliminaries

**LT-OOD setting.** Let  $\mathcal{D}_{\text{ID}} = \{(x_i, y_i)\}$  be a long-tailed training set with  $K$  ID classes and class counts  $\{n_c\}_{c=1}^K$ . At test time, a detector receives a query  $x$  and decides whether it comes from the ID distribution or from an unseen OOD distribution. We use the convention that larger OOD scores indicate samples that are more likely OOD.

**Energy score.** Given logits  $f(x) \in \mathbb{R}^K$  and temperature  $T > 0$ , the energy score is

$$\mathcal{E}(x) = -T \log \sum_{k=1}^K \exp(f_k(x)/T). \quad (1)$$

**Classifier row space and null space.** Let  $h(x) \in \mathbb{R}^d$  be the penultimate feature and let the linear classifier be  $f(h) = Wh + b$ , where  $W = [w_1^\top; \dots; w_K^\top] \in \mathbb{R}^{K \times d}$ . The classifier row space is  $\mathcal{R}(W^\top)$ , and its orthogonal complement is the classifier-null space  $\mathcal{N}(W) = \{v : Wv = 0\}$ . We use the orthogonal projectors

$$P_{\text{row}} = W^\top (WW^\top)^\dagger W, \quad P_{\text{null}} = I - P_{\text{row}}. \quad (2)$$

For any feature  $h = P_{\text{row}}h + P_{\text{null}}h$ , we have  $WP_{\text{null}}h = 0$ . Therefore,

$$f(h) = Wh + b = WP_{\text{row}}h + b = f(P_{\text{row}}h), \quad \mathcal{E}(h) = \mathcal{E}(P_{\text{row}}h). \quad (3)$$

Thus classifier scores, including Energy, are invariant to any perturbation that lies in the classifier-null component  $P_{\text{null}}h$ .

**Classifier-null absolute scatter.** To quantify the amount of feature variation that Energy cannot observe, we measure the within-class scatter that lies in the classifier-null subspace. For class  $c$ , let

$$\hat{\mu}_c = \frac{1}{n_c} \sum_{i:y_i=c} h_i, \quad \hat{\Sigma}_c = \frac{1}{n_c - 1} \sum_{i:y_i=c} (h_i - \hat{\mu}_c)(h_i - \hat{\mu}_c)^\top. \quad (4)$$

We define the absolute classifier-null scatter as

$$A_c^{\text{null}} = \text{Tr}(P_{\text{null}}\hat{\Sigma}_c P_{\text{null}}) = \frac{1}{n_c - 1} \sum_{i:y_i=c} \|P_{\text{null}}(h_i - \hat{\mu}_c)\|_2^2. \quad (5)$$

This quantity is an absolute trace rather than a fraction. It measures how much class-conditional variation is hidden from classifier scores, not just what proportion of the total scatter lies in the null space. For a group of classes  $\mathcal{G}$ , such as head or tail classes, we report

$$A_{\mathcal{G}}^{\text{null}} = \frac{1}{|\mathcal{G}|} \sum_{c \in \mathcal{G}} A_c^{\text{null}}. \quad (6)$$

## 4 Diagnosing and Repairing Long-Tailed Mahalanobis Geometry

### 4.1 Energy has a classifier-null blind spot

Let  $h(x) \in \mathbb{R}^d$ , logits  $f(x) = Wh(x) + b$ , and

$$\mathcal{E}(x) = -T \log \sum_{c=1}^K \exp(f_c(x)/T). \quad (7)$$

For any  $\delta \in \text{null}(W)$ ,  $W(h + \delta) + b = Wh + b$ . Thus Energy observes only classifier-visible coordinates. It can be strong when OOD evidence is classifier-aligned, but it is blind to classifier-null feature variation.

### 4.2 Raw Mahalanobis mixes feature radius with geometry

For raw features  $h = ru$ ,  $r = \|h\|_2$ , and  $\|u\|_2 = 1$ ,

$$\text{Cov}(h) = \mathbb{E}[r^2 uu^\top] - \mathbb{E}[ru]\mathbb{E}[ru]^\top. \quad (8)$$

When  $r$  is coupled with class frequency, raw Mahalanobis mixes semantic displacement with a long-tail nuisance coordinate. We score in hyperspherical coordinates  $z = h/\|h\|_2$  to remove this radius term before computing distances.

### 4.3 Tail classes cannot support class-specific covariance

A class-specific covariance in  $d$  dimensions has

$$\text{rank}(\hat{\Sigma}_c) \leq n_c - 1. \quad (9)$$

For tail classes,  $n_c \ll d$  is common, so full class-specific precision estimates have little support. HPM keeps class means specific but pools second-order geometry.

---

**Algorithm 1** HPM post-hoc OOD scoring. The algorithm normalizes frozen ID and query features, estimates class anchors with a pooled ridge covariance, and returns a Mahalanobis score where larger values indicate more OOD-like samples.

---

**Require:** Frozen encoder  $h(\cdot)$ ; ID training set  $\{(x_i, y_i)\}_{i=1}^N$  with labels  $y_i \in \{1, \dots, K\}$ ; query sample  $x$ ; ridge penalty  $\lambda > 0$ .

**Ensure:** Post-hoc OOD score  $s_{\text{HPM}}(x)$  (larger implies more OOD-like).

- 1: Collect training features  $\{h_i\}_{i=1}^N$  with  $h_i \leftarrow h(x_i)$  and the query feature  $h \leftarrow h(x)$ .
  - 2: Project onto the hypersphere  $z_i \leftarrow h_i / \|h_i\|_2$  and  $z \leftarrow h / \|h\|_2$ .
  - 3: Estimate class anchors  $\{\hat{\mu}_c^z\}_{c=1}^K$  and pooled ridge covariance  $\hat{\Sigma}_{\text{HPM}}$  exactly as in Theorem 1.
  - 4: **return**  $s_{\text{HPM}}(x) = \min_{c \in [K]} (z - \hat{\mu}_c^z)^\top \hat{\Sigma}_{\text{HPM}}^{-1} (z - \hat{\mu}_c^z)$ .
- 

#### 4.4 Why hyperspherical projection and pooled covariance repair the metric

**Lemma 1** (Pooled covariance expands supported directions). Assume  $n_c \geq 2$  for each class. Let

$$\hat{\mu}_c^z = \frac{1}{n_c} \sum_{i:y_i=c} z_i, \quad \hat{\Sigma}_c^z = \frac{1}{n_c - 1} \sum_{i:y_i=c} (z_i - \hat{\mu}_c^z)(z_i - \hat{\mu}_c^z)^\top, \quad (10)$$

let  $S_c = \text{span}\{z_i - \hat{\mu}_c^z : y_i = c\}$ , and let

$$\hat{\Sigma}_{\text{pool}} = \sum_{c=1}^K \alpha_c \hat{\Sigma}_c^z, \quad \alpha_c > 0, \quad \sum_c \alpha_c = 1. \quad (11)$$

Then

$$\text{range}(\hat{\Sigma}_{\text{pool}}) = \text{span}\left(\bigcup_{c=1}^K S_c\right). \quad (12)$$

With ridge regularization,  $\hat{\Sigma}_{\text{pool}} + \lambda I \succ 0$  for any  $\lambda > 0$ .

**Theorem 1** (HPM as stabilized Mahalanobis geometry). Assume  $N > K$  and  $n_c \geq 2$  for each class. Let  $z = h / \|h\|_2$  and define

$$\hat{\Sigma}_{\text{HPM}} = \frac{1}{N - K} \sum_{c=1}^K \sum_{i:y_i=c} (z_i - \hat{\mu}_c^z)(z_i - \hat{\mu}_c^z)^\top + \lambda I, \quad \lambda > 0. \quad (13)$$

Then HPM uses normalized class means as semantic anchors, removes raw feature radius before covariance estimation, and replaces tail-specific covariance with pooled residual geometry. Lemma 1 characterizes the covariance support before ridge regularization; after adding  $\lambda I$ , the precision is full-rank, with residual-supported directions shaped by the pooled covariance and orthogonal directions controlled only by the isotropic ridge.

The result is a mechanism statement rather than a universal dominance claim.

#### 4.5 The repaired detector

Given the normalized class means and pooled ridge covariance above, the OOD score is

$$s_{\text{HPM}}(x) = \min_c \left( \frac{h(x)}{\|h(x)\|_2} - \hat{\mu}_c^z \right)^\top \hat{\Sigma}_{\text{HPM}}^{-1} \left( \frac{h(x)}{\|h(x)\|_2} - \hat{\mu}_c^z \right). \quad (14)$$

## 5 Experiments

### 5.1 Setup

**Datasets and models.** We evaluate on CIFAR-10-LT, CIFAR-100-LT [Krizhevsky, 2009], and ImageNet-100-LT [Liu et al., 2019, Russakovsky et al., 2015]. The CIFAR-LT OOD suite follows common OOD benchmarks [Yang et al., 2022], covering digit [Netzer et al., 2011], texture [Cimpoi

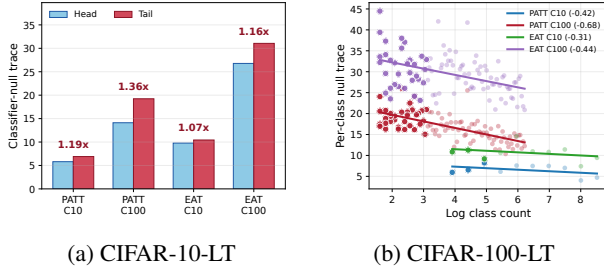


Figure 2: Classifier-null scatter in CIFAR-LT.

Table 1: **Mahalanobis variants.** Feature normalization and covariance estimation choices for the four post-hoc distance scores.

Name	Feature	Covariance
Mahalanobis	raw	class-specific
RP-MD	raw	pooled
HC-MD	hyperspherical	class-specific
HPM	hyperspherical	pooled

et al., 2014], scene [Yu et al., 2015], and object-level shifts; ImageNet-100-LT uses held-out ImageNet classes as near-OOD samples. CIFAR baselines include PATT [He et al., 2025], PASCL [Wang et al., 2022b], DARL [Zhang et al., 2025], AdaptOD [Miao et al., 2024b], COCL [Miao et al., 2024a], EAT [Wei et al., 2024], and PC-ERM. For methods originally trained with outlier exposure (OE), we report both the original checkpoint and the matched no-OE variant when available. PC-ERM uses the same backbone family and 200-epoch CIFAR budget, but only standard cross-entropy plus long-tail log-prior adjustment [Menon et al., 2021]; it has no auxiliary OOD data, outlier head, contrastive OOD objective, or detector-specific training loss.

**Scores and unified post-hoc protocol.** We compare Energy, maximum softmax probability (MSP), standard Mahalanobis, raw pooled Mahalanobis (RP-MD), hyperspherical class-specific Mahalanobis (HC-MD), and HPM under a common post-hoc OOD averaging protocol. For CIFAR-LT, we average over the OOD sets listed above. OOD detection is reported with area under the receiver operating characteristic (AUROC) and false positive rate at 95% true positive rate (FPR95); higher AUROC and lower FPR95 are better. ACC denotes closed-set ID classification accuracy. We also report LES,

$$\text{LES} = \lg \left( \frac{\text{BestAUROC}}{\text{Cost}} \right). \quad (15)$$

where BestAUROC is the strongest AUROC in the row and Cost is the model training time.

**Mahalanobis variants.** Let  $\mu_c$  be the feature mean of class  $c$ . A Mahalanobis detector scores a query by

$$s(x) = \min_c (z(x) - \mu_c)^\top \Sigma_c^{-1} (z(x) - \mu_c), \quad (16)$$

where  $z(x)$  may be the raw feature  $h(x)$  or its normalized version  $h(x)/\|h(x)\|_2$ , and  $\Sigma_c$  may be class-specific or pooled across classes. Table 1 summarizes the four post-hoc variants. Our method is HPM, which combines hyperspherical projection with pooled covariance.

## 5.2 Classifier-null blind spot

The following diagnostics explain why the same frozen representation can lead to different conclusions under classifier-score and feature-space detectors. Energy is computed only from classifier logits, so it cannot respond to variation orthogonal to the classifier row space. Figure 2 measures this blind spot in CIFAR-LT checkpoints: tail classes often carry larger classifier-null scatter than head classes, and the null-space component varies systematically with class count.

This result does not say that classifier scores are weak. Instead, it identifies a channel they cannot read. When OOD evidence is aligned with the classifier, Energy or MSP can be strong; when evidence lies in classifier-null variation, a feature-space detector has access to information that classifier outputs discard.

## 5.3 Feature-radius coupling

Figure 3 shows the radius-frequency coupling behind hyperspherical projection. Across representative checkpoints, raw feature norms increase from head to tail groups; for example, the tail/head ratio ranges from about 1.13 to 1.49 in the plotted cases. Thus raw Mahalanobis can treat class-frequency-induced radius variation as part of the distance geometry.

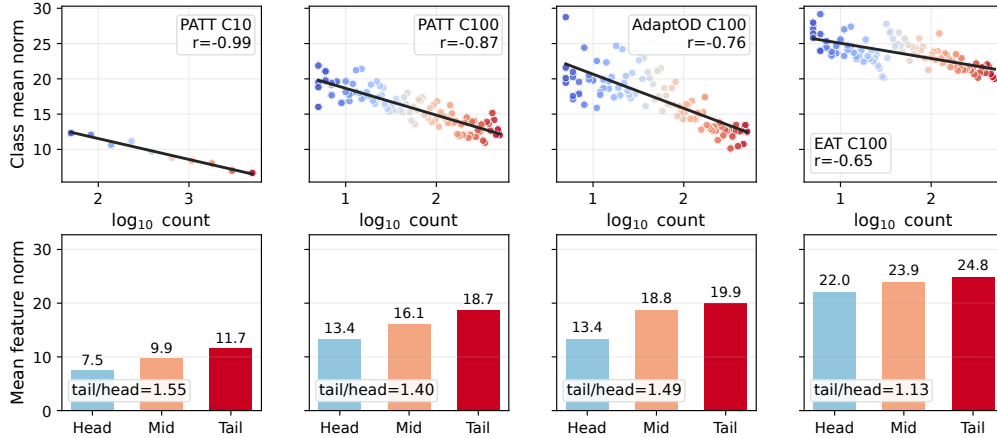


Figure 3: **Feature radius tracks class frequency.** Per-class backbone-feature norm versus training frequency across representative CIFAR-LT checkpoints used in the main tables. Larger norms for lower-frequency classes indicate that raw covariance is fit in coordinates where radius is coupled to imbalance, motivating the hyperspherical projection used before scoring.

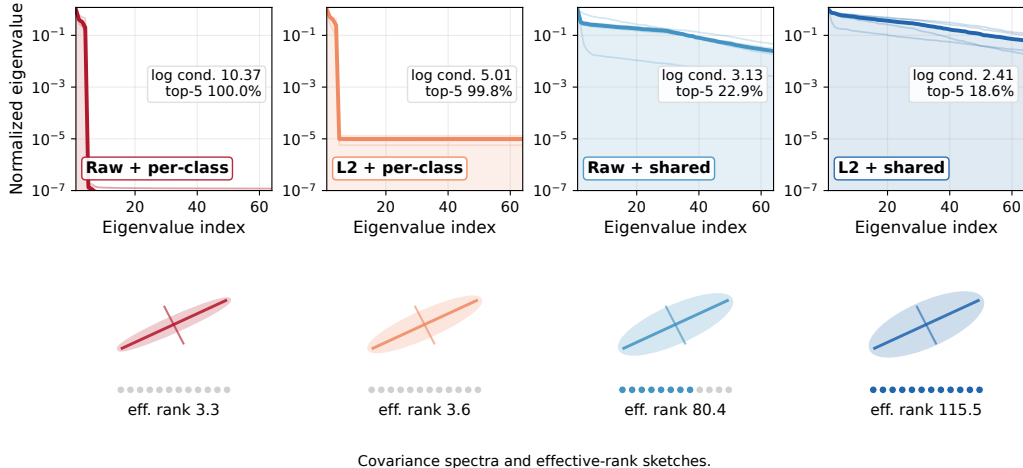


Figure 4: **Pooled hyperspherical covariance is better supported.** Four Mahalanobis variants on CIFAR-100-LT feature banks. Top: eigenvalues of the quadratic form, where sharp drops indicate dependence on a few dominant axes. Bottom: elliptical level sets with effective-rank and conditioning summaries; higher effective rank and lower condition number indicate better-supported geometry.

This explains why feature-space detection still needs repair. A larger radius for rare classes is not necessarily semantic OOD evidence; it can be a training artifact of long-tailed supervision. Hyperspherical projection removes this radial degree of freedom before covariance estimation, forcing the score to compare angular residual structure rather than raw norm scale.

#### 5.4 Covariance distortion

Figure 4 shows the second failure mode: raw per-class covariance is dominated by a few unstable directions. Across PATT, PC-ERM, DARL, and PASCL on CIFAR-100-LT, the median effective rank rises from about 3.3 for raw per-class covariance to about 115.5 for pooled hyperspherical covariance, while the median log-condition number drops from about 10.4 to about 2.4.

The comparison isolates the role of the two design choices in Table 1. Hyperspherical projection removes the radial nuisance identified in Figure 3; pooling then replaces tail-specific covariance estimates with residual directions shared across classes. This is consistent with Lemma 1: pooling

Table 2: **CIFAR-10-LT post-hoc OOD results.** Entries are averaged AUROC/FPR95; detector columns mark row-wise best/second-best values, ACC/LES are column-wise, and only top-three HPM cells are shaded.

Model	Energy	MSP	Mahalanobis	RP-MD	HC-MD	HPM	ACC	LES <sup>†</sup>
<i>Models trained with auxiliary outlier exposure.</i>								
PATT	81.78/51.29	<b>86.25/46.39</b>	46.61/87.99	56.80/76.80	82.76/47.57	85.20/44.28	79.86	1.96
AdaptOD	66.72/72.49	67.36/74.30	55.07/84.78	58.98/86.13	72.97/68.10	<b>77.75/62.88</b>	57.57	2.84
COCL	<b>89.75/42.17</b>	88.21/46.08	62.31/65.99	89.04/42.44	87.75/43.32	89.20/41.93	80.08	2.84
EAT	78.29/59.07	<b>79.57/60.21</b>	61.31/83.54	60.40/83.07	74.14/66.20	70.22/71.57	79.50	1.83
<i>Models trained without auxiliary outlier exposure.</i>								
PATT	<b>90.17/36.17</b>	87.47/40.06	58.28/76.70	55.30/78.17	85.44/43.34	86.78/41.05	83.01	1.97
PASCL	87.08/42.48	83.53/46.15	66.01/76.59	66.09/76.80	82.38/49.27	<b>88.89/40.29</b>	85.78	2.40
DARL	77.20/66.26	83.78/54.22	34.28/90.57	55.20/86.60	76.39/53.49	<b>88.72/38.15</b>	<b>87.71</b>	2.48
AdaptOD	73.87/64.66	69.48/67.98	66.98/77.81	57.79/81.70	78.52/61.51	<b>79.36/59.54</b>	66.58	2.87
COCL	<b>76.38/59.63</b>	74.15/61.11	72.04/65.71	59.36/76.31	72.86/60.71	70.58/67.03	76.81	2.79
EAT	65.39/80.19	64.34/79.98	66.50/82.82	55.82/82.95	<b>68.16/74.35</b>	65.58/78.49	73.40	1.77
PC-ERM	85.06/50.50	81.32/50.56	46.49/92.15	45.39/90.61	77.65/53.60	<b>85.67/46.38</b>	84.09	<b>3.05</b>

Table 3: **CIFAR-100-LT post-hoc OOD results.** Same protocol and notation as Table 2.

Model	Energy	MSP	Mahalanobis	RP-MD	HC-MD	HPM	ACC	LES <sup>†</sup>
<i>Models trained with auxiliary outlier exposure.</i>								
PATT	73.86/57.89	78.73/53.96	65.30/70.76	44.13/90.77	75.72/58.08	<b>81.41/46.81</b>	48.22	2.03
AdaptOD	<b>67.22/73.76</b>	59.85/84.38	43.84/92.25	44.55/91.80	57.24/83.94	51.42/89.33	32.98	2.80
COCL	<b>73.46/68.85</b>	71.03/72.49	44.98/93.28	65.93/75.57	68.91/71.93	71.40/69.95	45.10	2.77
EAT	<b>68.04/75.26</b>	62.97/82.20	57.19/89.57	58.03/85.57	62.92/81.10	63.39/83.81	43.70	1.80
<i>Models trained without auxiliary outlier exposure.</i>								
PATT	80.29/52.72	79.75/55.40	70.79/71.07	41.33/92.46	76.13/60.38	<b>82.61/45.56</b>	51.33	2.03
PASCL	76.20/64.42	70.74/72.87	55.71/88.75	54.16/89.30	73.64/64.55	<b>79.30/58.46</b>	50.88	2.43
DARL	62.17/78.50	68.54/74.88	53.95/90.93	47.33/93.39	69.64/71.15	<b>79.31/59.35</b>	<b>56.63</b>	2.25
AdaptOD	70.96/71.68	65.20/78.56	61.27/82.52	40.59/95.10	69.02/74.84	<b>72.82/69.86</b>	35.86	2.86
COCL	70.04/72.35	66.22/77.32	42.21/93.50	52.29/84.81	69.36/74.41	<b>76.86/66.57</b>	45.99	2.82
EAT	63.60/81.13	61.76/83.14	60.77/85.63	52.55/89.40	65.50/76.72	<b>70.09/75.21</b>	41.39	1.82
PC-ERM	73.44/67.64	67.96/73.05	50.40/91.26	54.81/90.77	71.95/66.46	<b>78.35/56.92</b>	51.91	<b>3.08</b>

does not create new features, but it aggregates complementary residual support; empirically, this produces a better-conditioned metric in Figure 4.

**Outlier exposure as a side analysis.** We treat OE as a side analysis rather than as the main target. Controlled no-OE/light-OE comparisons show that OE changes ID compactness, classifier-null variation, and radius-covariance coupling. Thus an OOD objective can improve a task-specific score without necessarily producing cleaner post-hoc geometry; this motivates reporting detector behavior on the same frozen checkpoints in the main tables.

## 5.5 CIFAR-LT results

Tables 2 and 3 compare six post-hoc scores on the same frozen CIFAR-LT representations. This tests when HPM repairs raw Mahalanobis scoring and when the repaired feature-space detector remains competitive with classifier scores.

**Result analysis.** HPM substantially improves raw Mahalanobis in most rows and is the best detector for all no-OE CIFAR-100-LT rows. Energy and MSP remain stronger in some CIFAR-10-LT or OE-trained cases, showing that classifier evidence and repaired feature geometry are complementary. For PC-ERM, HPM is best on both CIFAR datasets, raising raw Mahalanobis from 46.49 to 85.67 AUROC on CIFAR-10-LT and from 50.40 to 78.35 AUROC on CIFAR-100-LT, while also giving the highest LES. Figure 5 shows that this simple classifier retains roughly 95% of the best CIFAR-100-LT AUROC observed among the compared post-hoc scores with much lower training-time cost.

## 5.6 ImageNet-100-LT near-OOD analysis

Table 4 compares raw Mahalanobis with HPM on ImageNet-100-LT. Raw Mahalanobis remains consistently weak, while HPM substantially repairs feature-space scoring. This makes ImageNet-100-LT a boundary case for how much stabilization alone can recover from the raw Mahalanobis detector.

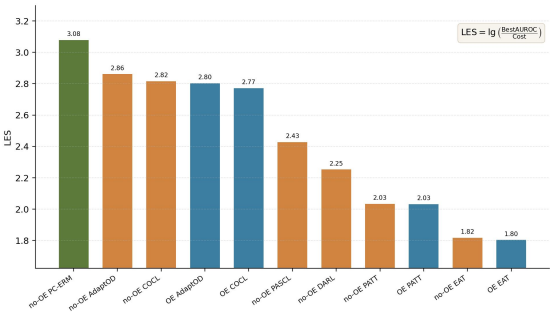


Figure 5: **CIFAR-100-LT efficiency.** LES compares best AUROC with training time; higher is better.

Table 4: **ImageNet-100-LT near-OOD.** Main AUROC/FPR95 comparison of Mahalanobis and HPM.

Model	Mahalanobis	HPM	ACC	LES $\uparrow$
<i>Models trained with auxiliary outlier exposure.</i>				
PATT	46.73/93.03	<b>81.04/54.33</b>	59.70	0.97
COCL	41.74/90.34	<b>81.45/59.35</b>	42.45	1.96
EAT	57.36/91.26	<b>80.18/63.43</b>	39.35	1.67
<i>Models trained without auxiliary outlier exposure.</i>				
PATT	40.99/95.65	<b>80.04/54.97</b>	55.60	0.95
COCL	35.26/95.96	<b>77.70/60.22</b>	41.20	1.97
EAT	50.47/95.29	<b>74.92/66.76</b>	38.70	1.64
PASCL	43.17/95.96	<b>88.26/37.88</b>	<b>66.30</b>	1.04
PC-ERM	52.85/89.42	<b>63.47/84.14</b>	46.40	<b>2.42</b>

## 6 Discussion and Limitations

Energy is effective when OOD separation is visible to the classifier, while HPM reads evidence that becomes usable after stabilizing feature geometry. LT-OOD performance should therefore separate the representation, the detector, and the cost paid to train the model.

PC-ERM suggests that gains from specialized LT-OOD training should be re-evaluated against simple training plus repaired post-hoc geometry. Auxiliary OOD data, extra heads, contrastive losses, energy regularization, and gradient-conflict mitigation can help, but in several CIFAR comparisons the gap narrows once detector geometry is stabilized. With only cross-entropy, long-tail prior calibration, and HPM, PC-ERM remains competitive on CIFAR-LT and obtains the best LES in both condensed CIFAR comparisons. On CIFAR-100-LT, it retains about 95% of the best AUROC observed among the compared post-hoc scores while achieving the highest LES. HPM is not a universal substitute for training-time objectives. ImageNet-100-LT remains a boundary case for stabilized Mahalanobis geometry: HPM repairs raw Mahalanobis substantially, but this repair alone does not settle all near-OOD settings. Our results instead argue that new objectives should justify their added complexity against simple baselines such as PC-ERM, stable post-hoc geometry, and efficiency metrics such as LES.

## 7 Conclusion

We revisited whether strong LT-OOD detection requires increasingly complex training. Raw class-specific Mahalanobis distance is distorted by feature-radius nuisance and unsupported tail covariance, so a simple classifier can be underrated when evaluated with an unstable feature-space metric. HPM addresses this geometry without auxiliary OOD data, retraining, or a new objective. Paired with simple PC-ERM, this repair yields competitive OOD performance and high LES, showing that new LT-OOD objectives should justify their added cost against stable post-hoc geometry. Code is available at <https://anonymous.4open.science/r/Neurips-26-DE01/>.

## References

Kaidi Cao, Colin Wei, Adrien Gaidon, Nikos Arechiga, and Tengyu Ma. Learning imbalanced datasets with label-distribution-aware margin loss. In *Advances in Neural Information Processing Systems*, 2019.

- Mircea Cimpoi, Subhansu Maji, Iasonas Kokkinos, Sammy Mohamed, and Andrea Vedaldi. Describing textures in the wild. In *IEEE/CVF Conference on Computer Vision and Pattern Recognition*, 2014.
- Yina He, Lei Peng, Yongcun Zhang, Juanjuan Weng, Shaozi Li, and Zhiming Luo. Long-tailed out-of-distribution detection: Prioritizing attention to tail. In *Proceedings of the AAAI Conference on Artificial Intelligence*, volume 39, pages 3446–3454, 2025. doi: 10.1609/aaai.v39i3.32357.
- Dan Hendrycks and Kevin Gimpel. A baseline for detecting misclassified and out-of-distribution examples in neural networks. In *International Conference on Learning Representations*, 2017.
- Dan Hendrycks, Mantas Mazeika, and Thomas Dietterich. Deep anomaly detection with outlier exposure. In *International Conference on Learning Representations*, 2019.
- Bingyi Kang, Saining Xie, Marcus Rohrbach, Zhicheng Yan, Albert Gordo, Jiashi Feng, and Yannis Kalantidis. Decoupling representation and classifier for long-tailed recognition. In *International Conference on Learning Representations*, 2020.
- Simon Kornblith, Jonathon Shlens, and Quoc V. Le. Do better imagenet models transfer better? In *IEEE/CVF Conference on Computer Vision and Pattern Recognition*, 2019.
- Alex Krizhevsky. Learning multiple layers of features from tiny images. Technical report, University of Toronto, 2009.
- Kimin Lee, Kibok Lee, Honglak Lee, and Jinwoo Shin. A simple unified framework for detecting out-of-distribution samples and adversarial attacks. In *Advances in Neural Information Processing Systems*, 2018.
- Tianhong Li, Peng Cao, Yuan Yuan, Lijie Fan, Yuzhe Yang, Rogerio Feris, Piotr Indyk, and Dina Katabi. Targeted supervised contrastive learning for long-tailed recognition. In *IEEE/CVF Conference on Computer Vision and Pattern Recognition*, pages 6918–6928, 2022.
- Shiyu Liang, Yixuan Li, and Rayadurgam Srikant. Enhancing the reliability of out-of-distribution image detection in neural networks. In *International Conference on Learning Representations*, 2018.
- Weitang Liu, Xiaoyun Wang, John D. Owens, and Yixuan Li. Energy-based out-of-distribution detection. In *Advances in Neural Information Processing Systems*, 2020.
- Ziwei Liu, Zhongqi Miao, Xiaohang Zhan, Jiayun Wang, Boqing Gong, and Stella X. Yu. Large-scale long-tailed recognition in an open world. In *IEEE/CVF Conference on Computer Vision and Pattern Recognition*, 2019.
- Aditya Krishna Menon, Sadeep Jayasumana, Ankit Singh Rawat, Himanshu Jain, Andreas Veit, and Sanjiv Kumar. Long-tail learning via logit adjustment. In *International Conference on Learning Representations*, 2021.
- Wenjun Miao, Guansong Pang, Xiao Bai, Tianqi Li, and Jin Zheng. Out-of-distribution detection in long-tailed recognition with calibrated outlier class learning. In *Proceedings of the AAAI Conference on Artificial Intelligence*, volume 38, pages 4216–4224, 2024a. doi: 10.1609/aaai.v38i5.28217.
- Wenjun Miao, Guansong Pang, Jin Zheng, and Xiao Bai. Long-tailed out-of-distribution detection via normalized outlier distribution adaptation. In *Advances in Neural Information Processing Systems*, 2024b. doi: 10.52202/079017-4199.
- Yifei Ming, Yiyun Sun, Ousmane Dia, and Yixuan Li. CIDER: Exploiting hyperspherical embeddings for out-of-distribution detection. In *International Conference on Learning Representations*, 2023.
- Maximilian Müller and Matthias Hein. Mahalanobis++: Improving OOD detection via feature normalization. In *Proceedings of the 42nd International Conference on Machine Learning*, volume 267 of *Proceedings of Machine Learning Research*, pages 45151–45184. PMLR, 2025.

- Yuval Netzer, Tao Wang, Adam Coates, Alessandro Bissacco, Bo Wu, and Andrew Y. Ng. Reading digits in natural images with unsupervised feature learning. In *NIPS Workshop on Deep Learning and Unsupervised Feature Learning*, 2011.
- Vardan Papyan, X. Y. Han, and David L. Donoho. Prevalence of neural collapse during the terminal phase of deep learning training. *Proceedings of the National Academy of Sciences*, 117(40): 24652–24663, 2020.
- Jiawei Ren, Cunjun Yu, Shunan Sheng, Xiao Ma, Haiyu Zhao, Shuai Yi, and Hongsheng Li. Balanced meta-softmax for long-tailed visual recognition. In *Advances in Neural Information Processing Systems*, 2020.
- Olga Russakovsky, Jia Deng, Hao Su, Jonathan Krause, Sanjeev Satheesh, Sean Ma, Zhiheng Huang, Andrej Karpathy, Aditya Khosla, Michael Bernstein, Alexander C. Berg, and Li Fei-Fei. ImageNet large scale visual recognition challenge. *International Journal of Computer Vision*, 115(3):211–252, 2015.
- Vikash Sehwal, Mung Chiang, and Prateek Mittal. Ssd: A unified framework for self-supervised outlier detection. In *International Conference on Learning Representations*, 2021.
- Yiyou Sun, Chuan Guo, and Yixuan Li. React: Out-of-distribution detection with rectified activations. In *Advances in Neural Information Processing Systems*, 2021.
- Yiyou Sun, Yifei Ming, Xiaojin Zhu, and Yixuan Li. Out-of-distribution detection with deep nearest neighbors. In *International Conference on Machine Learning*, 2022.
- Haoqi Wang, Zhizhong Li, Litong Feng, and Wayne Zhang. Vim: Out-of-distribution with virtual-logit matching. In *IEEE/CVF Conference on Computer Vision and Pattern Recognition*, 2022a.
- Haotao Wang, Aston Zhang, Yi Zhu, Shuai Zheng, Mu Li, Alex J. Smola, and Zhangyang Wang. Partial and asymmetric contrastive learning for out-of-distribution detection in long-tailed recognition. In *Proceedings of the 39th International Conference on Machine Learning*, volume 162 of *Proceedings of Machine Learning Research*, pages 23446–23458. PMLR, 2022b.
- Tong Wei, Bo-Lin Wang, and Min-Ling Zhang. EAT: Towards long-tailed out-of-distribution detection. In *Proceedings of the AAAI Conference on Artificial Intelligence*, volume 38, pages 15787–15795, 2024. doi: 10.1609/aaai.v38i14.29508.
- Jingkang Yang, Pengyun Wang, Dejia Zou, Zitang Zhou, Kunyuan Ding, WENXUAN Peng, Hao Wang, Guangyao Chen, Bo Li, Yiyou Sun, et al. Openood: Benchmarking generalized out-of-distribution detection. *Advances in Neural Information Processing Systems Datasets and Benchmarks Track*, 2022.
- Fisher Yu, Yinda Zhang, Shuran Song, Ari Seff, and Jianxiong Xiao. LSUN: Construction of a large-scale image dataset using deep learning with humans in the loop. arXiv preprint arXiv:1506.03365, 2015.
- Xuan Zhang, Sinchee Chin, Jing-Hao Xue, Xiaochen Yang, and Wenming Yang. DARL: Mitigating gradient conflicts in long-tailed out-of-distribution learning. In *Proceedings of the 33rd ACM International Conference on Multimedia*, pages 6868–6877, 2025. doi: 10.1145/3746027.3755127.
- Jianggang Zhu, Zheng Wang, Jingjing Chen, Yi-Ping Phoebe Chen, and Yu-Gang Jiang. Balanced contrastive learning for long-tailed visual recognition. In *IEEE/CVF Conference on Computer Vision and Pattern Recognition*, pages 6908–6917, 2022.